III-V/SOI as a versatile platform for innovative hybrid lasers : from fast tunable lasers to multi-mode DFB comb-source lasers

Alexandre Shen
III-V Lab, a joint lab from Nokia, *Thales and CEA*
Nokia Bell Labs
1, avenue Augustin Fresnel
91767 Palaiseau Cedex, France
alexandre.shen@3-5lab.fr

Emmanuel Bourgon
III-V Lab, a joint lab from Nokia, *Thales and CEA*
Nokia Bell Labs
1, avenue Augustin Fresnel
91767 Palaiseau Cedex, France
emmanuel.bourgon@3-5lab.fr

Pierre Fanneau de La Horie
Nokia Networks France
12 rue Jean Bart
91300 Massy, France
pierre.fanneau_de_la_horie-clavier@nokia.com

Delphine Néel
III-V Lab, a joint lab from Nokia, *Thales and CEA*
Nokia Bell Labs
1, avenue Augustin Fresnel
91767 Palaiseau Cedex, France
delphine.neel@3-5lab.fr

Théo Vérolet
Nokia USA
171 Madison Avenue
New York, USA
theo.verolet@nokia.com

Joan Ramirez
III-V Lab, a joint lab from Nokia, *Thales and CEA*
Nokia Bell Labs
1, avenue Augustin Fresnel
91767 Palaiseau Cedex, France
joan.ramirez@3-5lab.fr

David Bitauld
III-V Lab, a joint lab from Nokia, *Thales and CEA*
Nokia Bell Labs
1, avenue Augustin Fresnel
91767 Palaiseau Cedex, France
david.bitauld@3-5lab.fr

Karim Hassan
CEA-Leti
Université Grenoble Alpes
F-38000 Grenoble, France
karim.hassan@cea.fr

Alfredo de Rossi
Thales Research & Technologies
1, avenue Augustin Fresnel
91767 Palaiseau Cedex, France
alfredo.derossi@thalesgroup.com

***Abstract* — We present a III-V/SOI platform using wafer-bonding which allows integration of lasers. We demonstrated new lasers leveraging innovations this platform provides: nanosecond wavelength tuning laser, 10GHz-frequency continuous tuning DFB laser and a new few mode-locking laser.**

Keywords—Silicon Photonics, tunable laser, DFB laser, mode locking, frequency comb

I. Introduction

The silicon integration platform has shown to be gradually taking a leading position for the fabrication of low-cost and high volume photonic integrated circuits (PIC) [1]. The key component that was difficult to realize in this technology was the laser source. Today, the III-V on Silicon on insulator (SOI) heterogeneously integrated platforms using wafer- or die-bonding seem have matured [2-3] from research topics to industrial development through establishment of accessible foundry services.

We will present briefly the III-V / SOI platform, which we developed in III-V Lab, in part II. Then we will show through several examples how such a platform gave us the opportunity to develop and demonstrate innovative devices, such as p-i-n phase shifters integrated in a tunable laser, replacing thermo-optical ones, which allowed faster wavelength tuning (part III); or a capacitor-based phase shifter, integrated below the DFB laser structure, which also allowed fast and continuous wavelength tuning, with quasi-zero energy consumption (part IV); and finally, the integration of a non-uniform Bragg grating in a laser structure, which allowed us to demonstrate a new concept of mode locking (part V).

II. III-V / Si platform

The technology we adopted in III-V Lab uses the bonding of III-V dies/wafers [3-5]. It exploits the highly efficient light emission and modulation properties of some direct-gap III-V semiconductor materials such as compounds based on GaAs and InP. In this approach, all active components such as lasers, SOAs and electro-absorption modulators [4] are collectively processed, enabling low-cost and high volume. Moreover, the alignment of active waveguides to the passive circuitry is only limited by the accuracy of lithography equipment.

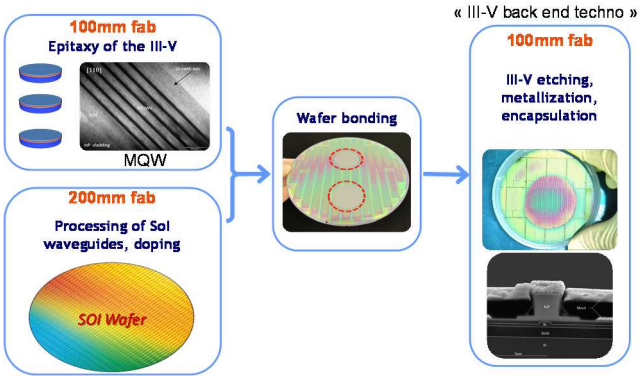

Fig. 1. III-V/Si platform, developed in III-V Lab.

Figure 1 shows the sequence of processing of the III-V/Si PICs on our platform. The III-V materials (MQW) are epitaxied in parallel with the SOI processing. Then the III-V wafers (or dies) are bonded on the processed SOI wafer thanks

to van der Waals interaction between the InP surface molecules and the thin silica bonding layer on top of the processed SOI. Then the InP substrate is removed and III-V backend processing performed, which includes ridge etching, metallization and encapsulation of devices.

Figure 2 shows a more complicated III-V/SOI fabrication process, including a backside processing stage (steps A to D): including 30nm-deep Bragg grating (BG) etching (A), Si carrier bonding (B), then wafer flipping and Si substrate grinding & etching (C), rib & or strip waveguide etching (D); followed by III-V on SOI wafer bonding (E), and eventually the above-mentioned III-V backend processing. We should point out here that we carried out a particular development to ensure a thin (20nm) yet very homogeneous SiO_2 bonding layer, allowing a net improvement to state-of-the-art methods [10].

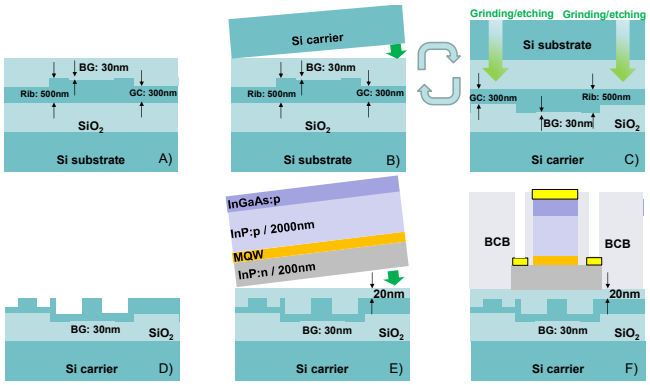

Fig. 2. SOI back side wafer processing (A to D), heterogeneous molecular bonding of III-V on SOI (E) & front side backend III-V processing (F)

III. P-I-N BASED FAST TUNABLE LASER

A. Hybrid III-V on Silicon Laser Structure

We fabricated the hybrid tunable laser in the III-V/Si platform described in part II, by wafer bonding a III-V active material on top of a SOI wafer. The III-V medium provides the optical gain of the laser, and Silicon forms the passive parts of the cavity. We used an adiabatic taper to couple the light from the Silicon waveguide to the III-V medium. Figure 3 presents a schematic of the tunable laser. The hybrid laser comprises a 100% back mirror, a 600 µm long active section, a fast tunable filter selecting one Fabry-Perot (FP) mode, a 20% output mirror, and a vertically emitting grating coupler.

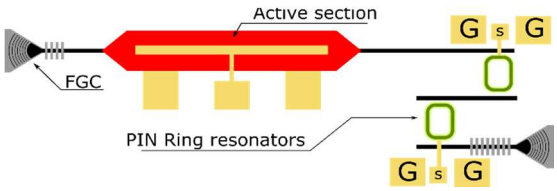

Fig. 3. Schematic of the tunable laser.

The tunable filter of a state of the art III-V/Si tunable laser is made of two RRs in a Vernier configuration, and thermally tuned. Because thermal effect has a response time in the micro second timescale [3], there is a real need to switch to a faster tuning mechanism for the mode selecting filter.

B. Fast Tunable Rings Resonators

Carrier injection in a silicon waveguide changes its refractive index through free carrier absorption and plasma dispersion effect (PDE) [6]. The cross section of the RR waveguide is sketched in Figure 4. The PIN junction can provide a refractive index change $\Delta n \sim n_f \Delta N$ with a n_f value of 2.1×10^{-21} cm^3 for an injection of ΔN carrier density in the range of 10^{18} cm^{-3} [7]. Thanks to the PIN junction the extra optical losses due to doping are avoided because the overlap integral between the optical mode and the doped regions is negligible. We measured a finesse of both RRs greater than 9.

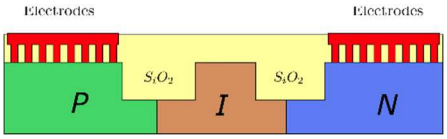

Fig. 4. Cross section of the RR rib waveguide.

C. Tunable laser characterization & fast wavelength switching demonstration

Spectra for different voltages applied on one RR PIN junction are displayed in figure 5. The measurement was done at 20°C, with a 100mA bias applied on the gain medium. When a forward biased is applied on one RR PIN junction, the injected carriers slightly shift the transmission spectrum of the RR due to PDE. By Vernier effect, the resonance peak of the double ring filter will hop from one resonance of the second ring resonator to the adjacent resonance. So the Vernier filtering will select another FP mode, and the output wavelength of the laser will be modified. The maximum tuning range of 45nm imposed by the Vernier filter is reached. For every operating point we measured a SMSR greater than 40dB. We can notice that the device output power slightly decreases for higher wavelength, this is due to the fact that the vertical grating coupler has additional losses for higher wavelength.

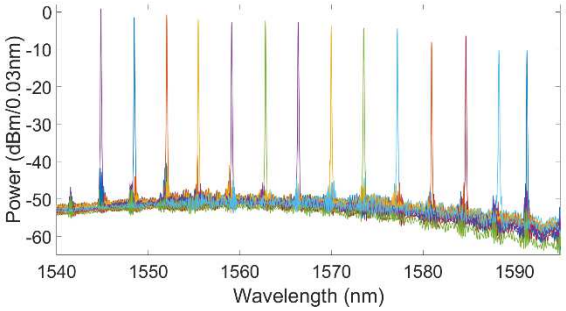

Fig. 5. Laser Spectra for different control voltage on one RR. The gain medium was biased at 100mA.

The experimental setup used for fast switching characterization of the laser is shown in figure 5. Firstly one of the RR PIN junction is forward biased, $V_{DC} \sim 5V$. Then we applied V_{RF}, a square signal at 200 MHz with a 1V peak to peak voltage on the same junction. Thanks to the Vernier effect, the laser output wavelength will hop from λ_1 when V_{RF} is equal to -0.5V to λ_2 when V_{RF} is equal to 0.5V. $|\lambda_1 - \lambda_2|$ is the FSR of the second RR.

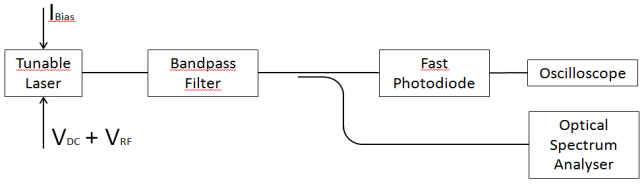

Fig. 6. Experimental setup to characterize the laser frequency switching. I_{bias} is the optical gain bias, V_{DC} is the forward bias of one PIN junction, V_{RF} is the square signal applied to the same PIN junction.

Then an external band pass optical filter with an attenuation of more than 20dB for one of the two possible laser output wavelengths is used to convert the binary frequency modulation into an amplitude modulation at the detector.

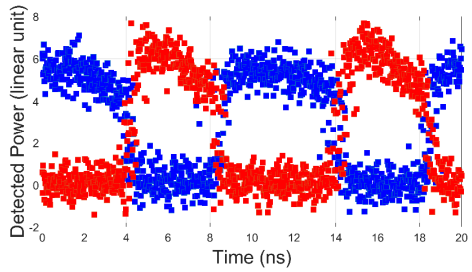

Fig. 7. Temporal response of the laser under modulation.

The amplitude-modulated signal is then detected by a fast photodiode and a sampling oscilloscope. Figure 7 plots the temporal response of the laser. The red curve is obtained when the optical filter is centered on λ_1 (1551.9 nm) and the blue curve when the filter is centered on λ_2 (1548.5 nm). The superposition of the curves shows the wavelength switching. We measure a rising and falling time below 1.5 ns. This result is 3 orders of magnitude faster that the result obtained with thermal tuning [3], and in the same order of magnitude as the result obtained within the monolithic InP platform [8].

D. Part III conclusion: fast tunable hybrid laser

We demonstrated a III-V on Silicon fast tunable laser for the first time [9]. It was achieved thanks to a fast tunable double ring Vernier filter using a PIN junction. The device vertically coupled output power is more than 1.5mW in a single mode fiber. The laser linewidth is lower than 500kHz, it is thus suited for coherent format transceiver applications. A tunability of 45nm was achieved. We showed a switching time lower than 1.5ns, thus this hybrid III-V on SOI hybrid laser is a promising solution for wavelength packet switching in the next generation Metro Networks.

IV. Capacitor-based fast and continuously tunable DFB laser

In this section, we present and demonstrate a new DFB laser with a hybrid capacitor integrated beneath the active MQW structure, between the III-V and the Si materials. Within the III-V / Si platform we presented in section I, we used a slightly modified process to fabricate this new laser.

A. Hybrid capacitor integration in the III-V/Si DFB laser

Figure 8 describes the vertical structure of this laser. It comprises an active III-V waveguide optically coupled to a passive Silicon waveguide allowing the light to propagate in a hybrid III-V/Si optical mode. The III-V structure is composed of multiple quantum wells (MQW), sandwiched between a top P-doped InP layer and a bottom N-doped InP one. What is new from our classical process is that the Silicon rib waveguide beneath the III-V film is P-doped silicon waveguide under a 23 nm thick SiO_2 oxide layer. The N-doped InP, SiO_2, thin silica layer and P-doped Si structure forms a hybrid semiconductor-insulator-semiconductor (SIS) capacity.

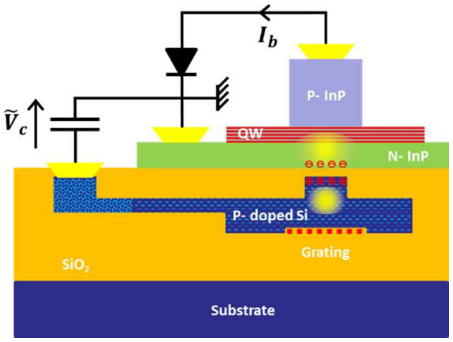

Fig. 8. Cross section of the hybridly integrated capacitor within the DFB laser structure.

Backside processing (section II, fig. 2) of the SoI wafer was used in order to etch the DFB grating far from the SIS carrier accumulation region. Accumulation of carriers in the SIS capacity alters the mode effective index through plasma dispersion, which induces continuous tuning of the lasing mode through the modification of the Bragg resonant condition. This provides a fast and energy efficient solution to perform wavelength tuning without current or temperature adjustments. The design of this device was inspired by the one used by Liang *et al.* [11].

B. Static tests of the hybrid capacitor-integrated DFB laser

We set the hybrid laser chip temperature at 20°C and applied a 100mA bias current on the gain section. Then we recorded the optical spectra from one of the laser output. Under these conditions, the laser emitted spectrum presents a single line at around 1539 nm (Fig. 9) with a side mode suppression ratio over 60 dB. The optical power coupled in fiber through grating couplers reaches 4.4mW at 175mA. To tune the optical frequency, we applied a forward bias to the hybrid capacitor, which induces a carrier accumulation at the semiconductor-oxide interfaces leading to a variation of the effective index.

We show this optical frequency shift in Fig. 9 and Fig. 10, for voltages varying from 0V to 7.5V, the frequency shift magnitude is 10 GHz. Since this frequency shift is driven by a capacitive effect, the static operation consumes only a maximum of 100pW induced by the leakage currents, which is negligible compared to other tuning mechanism such as thermo-optic effects.

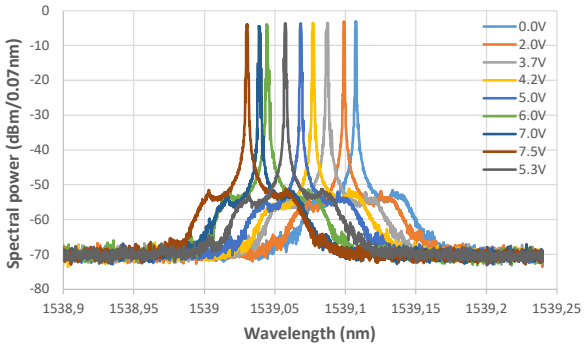

Fig. 9. Laser spectra for different bias voltage on the integrated capacitor

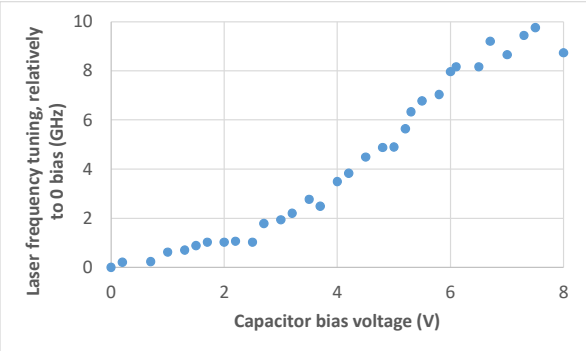

Fig. 10. Laser frequency tuning, relatively to 0 bias.

C. *Dynamic demonstration of the hybrid capacitor-integrated DFB laser*

We applied a radio frequency (RF) signal to the hybrid-capacitor-integrated DFB laser to study its frequency modulation (FM) response. We kept the capacitor in the accumulation regime, while biasing the gain section at 100mA and keeping its temperature regulated at 20 °C. Both small and large signal responses are measured using the methods of [12, 13]. The small signal FM responses plotted in Fig. 11, show a 3 dB bandwidth above 1 GHz for biases between 0 V and 5 V. These FM spectra present a peak around 3.5 GHz that we expect to be related to the DFB laser relaxation oscillation that extends the 6 dB bandwidth to 7 GHz.

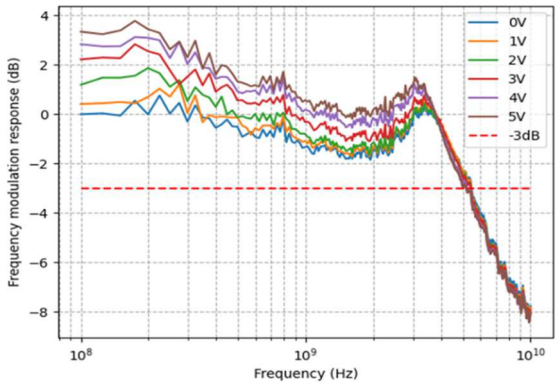

Fig. 11. Small signal FM response spectra for different forward biases voltage on the integrated hybrid capacitor

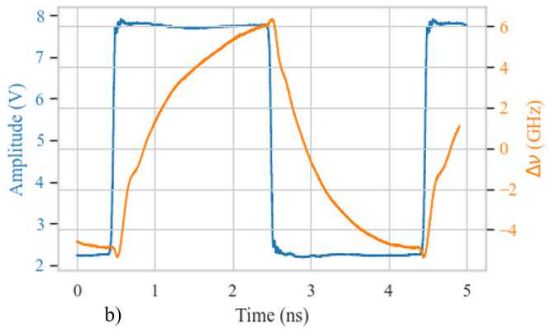

Fig. 12. Large signal FM response of the hybrid capacitor-integrated DFB laser to a square driving signal.

The laser FM large signal oscillogram plotted in Fig. 12 is obtained by applying a 250 MHz square signal of 5.7 V peak-to-peak voltage and 5 V offset. It shows that the DFB laser is continuously tunable across 10.9 GHz in a time below 2 ns. Switchable lasers in the nanosecond timescale have already been demonstrated [10, 14], but we demonstrated for the first time a continuous fast sweep of the lasing frequency [15]. One may notice a small parasitic peak on the FM response located at each edge of the driving signal. This peaking comes from the relaxation oscillation, amplifying high frequency harmonics of the square signal.

D. *Part III conclusion: hybrid capacitor-integrated DFB laser*

In this section, we reported on the ultra-fast continuous frequency sweep of a new III-V/Si capacitive DFB laser over a 10 GHz span. We have shown an original capacitive structure in the Si waveguide region beneath the III-V gain section, and demonstrated its efficient refractive index fast tuning functionality, for the first time, to our best knowledge. This proof of the concept paves the way for many application opportunities, such as fast switching of radio frequency in carrier signal generation through heterodyne schemes; fast continuously tunable local oscillator laser source for coherent communications, or as a subsystem enabling hardware carrier frequency offset correction.

V. DFB LASER-BASED A FEW LOCKED MODES COMB SOURCE

In this section, we present a laser cavity based on a tapered distributed feedback grating on Silicon, similar to the low-noise laser demonstrated Santis *et al.* [16, 17] Here the tapering profile is changed to allow a few equispaced modes, based on the concept of effective parabolic potential in a photonic crystal [18].

Compared with classical mode locked designs, namely Fabry-Perot (FP) cavity based mode locked lasers [19] and optically pumped ring resonators [20], this type of distributed feedback laser design offers design flexibility as the mode separation is no longer linked to active cavity free spectral range. Here we demonstrate a remarkably stable frequency comb over > 50 mA bias current range. Here, we demonstrate the first mode locking of an engineered photonic bandgap III-V on Silicon laser exhibiting narrow linewidth modes spaced by 28 GHz.

A. *Hybrid III-V/Si DFB laser : the concept of a new frequency comb source*

The device described in Fig 13 a) and b) is fabricated using a specific backside III-V on Silicon wafer bonding process, with a SiO_2 bonding layer as thin as 23 nm, as we described it in section II (fig. 2) and IV. 6 AlGaInAs quantum well layers provide optical gain. We chose Aluminum-based quantum wells because of their higher band offset in the conduction band than Phosphide-based ones. As a result, we obtain a much better electron confinement that decreases the thermionic emission, hence making them suitable for high temperature operation [21].

In order to achieve the desired value of grating strength, we etched the grating corrugation using a backside process developed in the CEA Leti's 200mm pilot line [10, 22]. The resulting average grating strength is around 81 cm^{-1}. The laser is 1.6 mm long and contains two gain sections separated by an isolating hydrogen implantation zone, allowing us to have an asymmetric current injection in the two halves of the laser gain medium. As previously stated, the design of the laser is inspired by Santis *et al* [16, 17]. Their motivation for an

engineered photonic bandgap laser was to control the spatial field distribution in order to reduce radiative and extraction losses leading to reduced phase noise of the single-mode laser. Our main feature in this section is to put several modes with minimum gain margin in the same type of cavity based on the engineered parabolic photonic well. This, produces -by design- a very stable and fabrication resistant laser frequency comb as predicted in [23] with equally spaced modes. Fig. 14 illustrates the parabolic photonic bandgap with the equivalent photonic valence and conduction bands and their corresponding lasing frequency levels. We computed the frequency levels from a transfer matrix simulation method (TMM) of the Bragg grating [24]. The photonic well is made by inducing a parabolic offset in the photonic valence band.

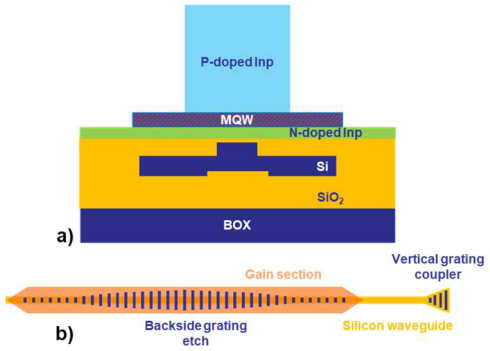

Fig. 13. a) Schematic cross-section of the laser b) simplified layout of the cavity

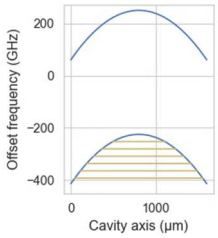

Fig. 14. Engineered photonic bandgap containing the different frequency levels.

We can thus optimize the modes gain margin by adjusting the well's length and depth. We implemented a longer and deeper photonic well than Santis' to achieve multimode lasing.

B. Characterization of the hybrid DFB-based frequency comb source

We performed all the measurements above 55°C in order to align both the optical gain peak and the engineered photonic bandgap frequency levels. The multi-section DFB laser exhibits a fiber coupled output power of 1mW for 230 mA bias current in both sections at a regulated temperature of 60°C.

Fig. 15 shows a typical optical spectrum, demonstrating a comb of four lasing frequencies. A current of 183mA biased both sections of the DFB laser. We kept the temperature of chipset at 60°C to ensure maximal gain for the lasing frequencies. In a next run, we will adjust the gain spectrum of the MQW material to improve the match with the lasing frequencies of the parabolic cavity.

Fig. 16 shows a mapping of the spectral power as a function of the bias current. We shall point out a large range of bias current (175mA to 225mA) for which the multi-frequency comb laser is very stable: the laser lines remain at their spectral positions and the free spectral range seems to be equal. Outside this bias range however, we observe frequency comb shift to lower frequencies. The overall spectral domain mapping with bias current varying in both sections is still under way in III-V Lab.

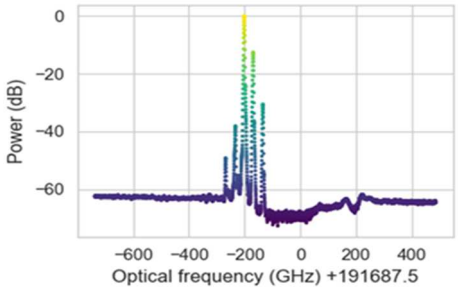

Fig. 15. A typical spectrum of the comb-laser source, the bias current is 183mA, the laser device is temperature regulated at 60°C.

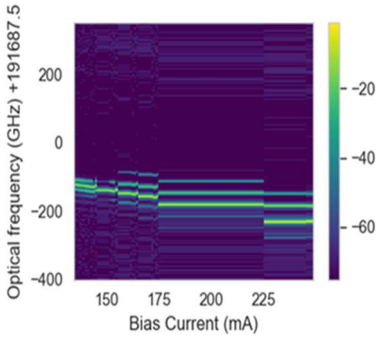

Fig. 16. Spectral power mapping as a function of the bias current, the laser device is temperature regulated at 60°C.

By driving one of the laser gain sections with a small (RF power around -1 dBm) sinusoidal signal at 28.5 GHz center frequency, it is possible to observe a stable mode locking of the laser characterized by a 20 kHz -3 dB bandwidth peak on the electrical spectrum (Fig 17 c) [26]. We clearly observe a mode locking regime, excluding any gain-switching one, as the driving signal power is too small to reach threshold (RF swing of 0.16mA across the laser diode of resistance 3.46 Ω injected with 183 mA DC bias). We also observed a frequency locking range. Its amplitude depends on the RF signal power, which is -1dBm here. The unresolved very fine peak at the top of Lorentzian-shaped microwave signal on Fig 17 c) spectrum is the signature of the sinusoidal driving signal.

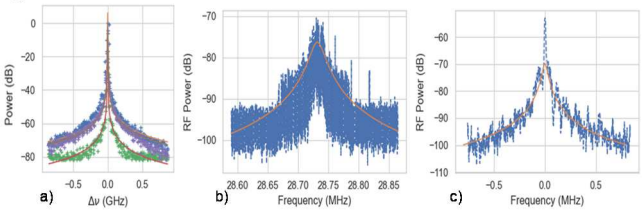

Fig. 17. a) Superposed optical spectra showing the spectral power vs lasing frequency offset of the well lasing modes. Lorentzian fit are computed to estimate their linewidth. b) RF spectrum under free running operation of the laser (100 kHz resolution bandwidth, 10 kHz video bandwidth). c) RF spectrum of the mode locked laser driven by a -1 dBm power 28.3 GHz sinusoidal signal (100 kHz resolution bandwidth, 10 kHz video bandwidth). Frequency offset is 28.3 GHz

C. *Part V conclusion: the hybrid DFB-based frequency comb source*

We demonstrated [26] the stable mode locking operation of a III-V on Si multimode laser exhibiting three narrow linewidths modes spaced by ~28 GHz over a large bias current range (>50 mA). Active locking of the modes is achieved by driving one of the two laser gain sections with a -1 dBm small electrical sinusoidal signal at the 28 GHz frequency. A 20 kHz wide beat tone is observed. This flexible and fabrication proof design paves the way for future applications requiring temperature-insensitive frequency combs in a diversity of fields, spanning telecommunications and datacommunications, metrology, sensing, among others. Further improvements of this laser structure include the use of quantum dots instead of quantum wells to enable passive mode-locking operations with a lower level of phase noise, and better insensitiveness to optical feedback [27]. In addition, a different design of the photonic bandgap would reduce modes extraction losses in order to achieve equalized power frequency comb teeth.

VI. Conclusion and Perspectives

We presented the III-V Lab silicon photonics platform incorporating the crucial III-V wafer- or die-bonding step, which allows the integration of III-V active devices on the silicon wafer. We have shown such a versatile technology platform allows technology innovations through three examples. 1/ Using p-i-n junction instead of TiPt heater in ring-resonator architecture allowed us to demonstrate a much faster wavelength-switching laser, with a characteristic time of just a few nanoseconds. 2/ Integrating a capacitor beneath a DFB laser granted the demonstration of a fast and continuous tuning of the laser frequency over more than 10GHz. 3/ A 2-section DFB laser in which the grating teeth width has a parabolic profile was the third innovation example we carried out to demonstrate a few locked modes laser; the frequency spacing is shown to be tunable with the bias current of the laser diode. These innovative demonstrations must now be developed into products for a variety of applications, such as wavelength packet switching, fast spectroscopy-based sensing, or WDM data communication. These innovations also pave the way to the development of laser devices with lower energy consumption.

Acknowledgment

The authors thank their colleagues, Claire Besançon, Nicolas Vaissière, Arnaud Wilk and Jean Decobert for having provided the epitaxy development of the III-V wafers; Valentin Ramez and Stéphane Malhouitre for having processed the SOI wafers and monitored the III-V on Si wafer-bonding; and Sylvain Combrié for technical assistance in the experimental work with the few mode locking of the DFB laser. European project H2020-ICT-2017 PICUTRE funded part of the work, under grant agreement n°780930.

References

[1] P. Dong, Y.-K. Chen, G.-H. Duan, and D. T. Neilson, “Silicon Photonic Devices and Integrated Circuits”, Invited paper, J. Nanophotonics, 2014.

[2] .G.-H. Duan et al., « Hybrid III-V on Silicon Lasers for Photonic Integrated Circuits on Silicon”, IEEE J. of Select. Topics in Q. Electron., Vol. 20, No. 4, 2014

[3] G.-H. Duan et al., " Hybrid III-V Silicon Photonic Integrated Circuits for Optical Communication Applications”, IEEE J. of Select. Topics in Q. Electron., Vol. 22, No. 6, 2016

[4] A. W. Fang et al., “Hybrid silicon evanescent devices”, Materials Today, vol. 10, Issues 7-8, p. 28-35, 2007.

[5] H. Park et al., “Device and Integration Technology for Silicon Photonic Transmitters”, IEEE J. of Selected Topics on Quantum Electronics,, vol. 17, No. 3, pp. 671-688, 2011.

[6] R. Soref and B. Bennett, “Electro-optical effects in silicon", IEEE Journal of Quantum Electronics, vol.23 no. 1,pp. 123, Jan 1987.

[7] R. Wu *et al*, “Compact models for carrier-injection silicon microring modulators”, Opt. Express **23**, 15545-15554 (2015)

[8] J R. O'Dowd, S. O'Duill, G. Mulvihill, N. O'Gorman and Yonglin Yu, “Frequency plan and wavelength switching limits for widely tunable semiconductor transmitters” in IEEE Journal of Selected Topics in Quantum Electronics, vol. 7, no. 2, pp. 259-269, March-April 2001.

[9] T. Verolet et al., “Hybrid III-V on Silicon Fast and Widely Tunable Laser Based on Rings Resonators with PIN Junctions”, ACP 2018

[10] Durel, J., et al. "First demonstration of a back-side integrated heterogeneous hybrid III-V/Si DBR lasers for Si-photonics applications." 2016 IEEE International Electron Devices Meeting (IEDM). IEEE, 2016.

[11] Liang, D. et al. Integrated finely tunable microring laser on silicon. Nature Photon 10, 719–722 (2016). https://doi.org/10.1038/nphoton.2016.163

[12] R. A. Saunders et al., "Wideband chirp measurement technique for high bit rate sources," in Electronics Letters, vol. 30, no. 16, pp. 1336-1338, 4 Aug. 1994, doi: 10.1049/el:19940917.

[13] J. Provost et al., "Measuring the Chirp and the Linewidth Enhancement Factor of Optoelectronic Devices with a Mach–Zehnder Interferometer," in IEEE Photonics Journal, vol. 3, no. 3, pp. 476-488, June 2011, doi: 10.1109/JPHOT.2011.2148194.

[14] Yuta Ueda et al., "Electro-optically tunable laser with ultra-low tuning power dissipation and nanosecond-order wavelength switching for coherent networks", Optica 7, 1003-1006 (2020)

[15] P. Fanneau de La Horie et al., "A nanosecond-tunable capacitive III-V/Si distributed feedback laser ", CLEO 2021

[16] C. T. Santis, et al., “Quantum control of phase fluctuations in semiconductor lasers.” 2018 Proceedings of the National Academy of Sciences, 201806716–. doi:10.1073/pnas.1806716115

[17] C. T. Santis, et al., “High-coherence semiconductor lasers based on integral high-Q resonators in hybrid Si/III-V platforms,” Proc. Natl. Acad. Sci. U. S. A., vol. 111, no. 8, pp. 2879–2884, 2014

[18] H. Kogelnik et al. “Coupled-Wave Theory of Distributed Feedback Lasers”, Journal of Applied Physics 43, 2327 (1972)–. doi:10.1063/1.1661499

[19] P J. Delfyett et al., "Optical Frequency Combs From Semiconductor Lasers and Applications in Ultrawideband Signal Processing and Communications," J. Lightwave Technol. 24, 2701- (2006) https://opg.optica.org/jlt/abstract.cfm?URI=jlt-24-7-2701

[20] P. Del’Haye et al., Optical frequency comb generation from a monolithic microresonator. Nature 450, 1214–1217 (2007)–. doi:10.1038/nature06401

[21] L. A. Coldren et al., . Diode lasers and photonic integrated circuits. John Wiley & Sons, 2012.

[22] D. Néel et al., "Novel technology of III-V die-bonded SOI photonic integrated circuits", Proc. SPIE 11880, Emerging Applications in Silicon Photonics II, 118800M (6 October 2021); https://doi.org/10.1117/12.2603190

[23] Y. Sun et al., "Robustness of mode-locking in harmonic cavity nanolasers subjected to potential distortions," Opt. Express 29, 5782-5794 (2021)

[24] G. Bjork et al., "A new exact and efficient numerical matrix theory of complicated laser structures: properties of asymmetric phase-shifted DFB lasers," in Journal of Lightwave Technology, vol. 5, no. 1, pp. 140-146, January 1987, doi: 10.1109/JLT.1987.1075402.

[25] A.E. Siegman, “Lasers” University Science Books 1986.

[26] P. Fanneau de La Horie et al., « Few-modes locking in a photonic bandgap III-V on Silicon Laser », ECOC 2022

[27] B. Dong et al., 1.3-µm passively mode-locked quantum dot lasers epitaxially grown on silicon: gain properties and optical feedback stabilization - IOPscience. 2020, Journal of Physics: Photonics, Volume 2, Number 4